Mapping of trap densities and energy levels in semiconductors using a lock-in infrared camera technique

Peter Pohl,[a] Jan Schmidt, Karsten Bothe, and Rolf Brendel
Institut für Solarenergieforschung Hameln/Emmerthal (ISFH), Am Ohrberg 1, 31860 Emmerthal, Germany

(Received 9 May 2005; accepted 9 August 2005; published online 28 September 2005)

We examine nonrecombination active minority-carrier trapping centers in crystalline silicon using a lock-in infrared camera technique. Application of a simple trapping model to the injection-dependent lifetime data obtained from the infrared emission signal results in high-resolution mappings (spatial resolution=170 μm) of the trap density and the energy level. Measurements on Czochralski-grown silicon wafers show striation-related inhomogeneities of the trap density and a very homogeneous distribution of energy levels. © *2005 American Institute of Physics*. [DOI: 10.1063/1.2077833]

The recombination lifetime of a semiconductor is a key parameter for electronic devices, such as bipolar transistors and solar cells. At low illumination levels, abnormally high apparent lifetimes, which should not be confused with the actual recombination lifetime, are frequently measured when minority-carrier trapping centers are present in a significant concentration.[1] For transient photoconductance decay measurements,[2,3] the relatively slow detrapping of minority carriers causes a long tail in the photoconductance decay curve pretending an extremely high lifetime.[4] Moreover, a significant impact of traps has also been observed on both the steady-state and the quasi-steady-state photoconductance of a semiconductor.[4] At excess carrier concentrations comparable to or below the trap density, charge neutrality implies that the presence of minority-carrier traps causes a relative increase in the concentration of majority carriers, leading to an increase in the steady-state photoconductance.[4] Recently, the quasi-steady-state photoconductance (QSSPC) (Ref. 5) technique has been used to characterize minority-carrier traps in silicon wafers.[4] The application of a simple theoretical model to QSSPC measurements allowed the determination of the most relevant trap parameters (trap density N_t, ratio of trapping/detrapping time constants τ_t/τ_d and trap energy level E_t).[4] However, the mentioned measurement techniques typically average over a sample area of a few cm^2, whereas a good spatial resolution would be highly desirable to characterize distributions of traps.

In this letter, we introduce a mapping technique for minority-carrier trapping centers in semiconductors based on lock-in infrared thermography. We term this method infrared trap mapping (ITM) as it is derived from the infrared lifetime mapping (ILM) technique introduced by Bail *et al.*,[6] which measures spatially resolved carrier lifetimes.[6–8] In our experimental setup, an infrared camera that is sensitive in the long-wavelengths range [peak sensitivity at wavelength $\lambda_{det}=(8.3\pm0.6)$ μm, frame rate 38.9 Hz, focal plane array with 640×486 detectors] images the semiconductor wafer that is heated to a constant temperature T_W in the range of 20–150 °C. In order to determine injection-dependent lifetimes, we generate excess carriers in the silicon wafer under test by means of a diode array ($\lambda_{ex}=880$ nm), which is periodically turned on and off. The photon flux is measured by a calibrated solar cell. The emission change at $\lambda_{det}=8.3$ μm is determined using lock-in technique as described in Ref. 9. We apply a low lock-in frequency (typically 0.1–2 Hz). Hence, the in-phase camera signal S_0 is used to calculate the lifetime since the excess carrier concentration is in phase with the illumination intensity. As our measurements are performed under steady-state conditions, we determine the apparent lifetime τ_a of the sample using the simple expression[8]

$$\tau_a = \frac{S_0}{m(1+\alpha_n/\alpha_p)gW}, \tag{1}$$

where g denotes the photogeneration rate in (cm^{-3} s^{-1}) of electron-hole pairs and W is the thickness of the sample. m is a proportionality factor, which has been measured using a set of p-type silicon wafers of different well-defined doping concentrations. Details of the calibration procedure are described elsewhere.[6] The correction factor $(1+\alpha_n/\alpha_p)$ includes the absorption coefficient for electrons α_n and holes α_p at the detection wavelength λ_{det} (Ref. 10) and accounts for the fact that under illumination electrons as well as holes are generated, whereas in our calibration procedure p-type silicon is used. According to Kirchhoff's law, the absorption coefficient always equals the emission coefficient $\alpha(\lambda)\equiv\epsilon(\lambda)$. Hence, the measurement can be performed in absorption or emission mode, depending on the temperature of the material under investigation and the temperature of the background. In this letter, we measure in emission mode, but Eq. (1) holds in both cases.

We apply the ILM technique to Czochralski silicon (Cz–Si) wafers [n-type 0.33 Ω cm, (100)-oriented, thickness 280 μm, interstitial oxygen concentration $[O_i]=1.3\times10^{18}$ cm^{-3}], which are cut into pieces of 2×2 cm^2. Both surfaces are passivated with 70 nm thick silicon nitride films deposited in a remote plasma-enhanced chemical vapor deposition system at 400 °C.[11]

Figure 1 shows three images of the infrared emission signal S_0 of the same Cz–Si sample at three different illumination intensities (10^{-5} suns, 10^{-2} suns, and 1 sun). As expected, the overall excess-carrier emission signal decreases with decreasing illumination intensity. Surprisingly, the qualitative appearance of the images completely changes with increasing illumination intensity, resulting in an anticorrelation of Fig. 1(b) with the other two images [Figs. 1(a) and 1(c)]. Figure 2 shows two examples of injection-

[a]Electronic mail: p.pohl@isfh.de

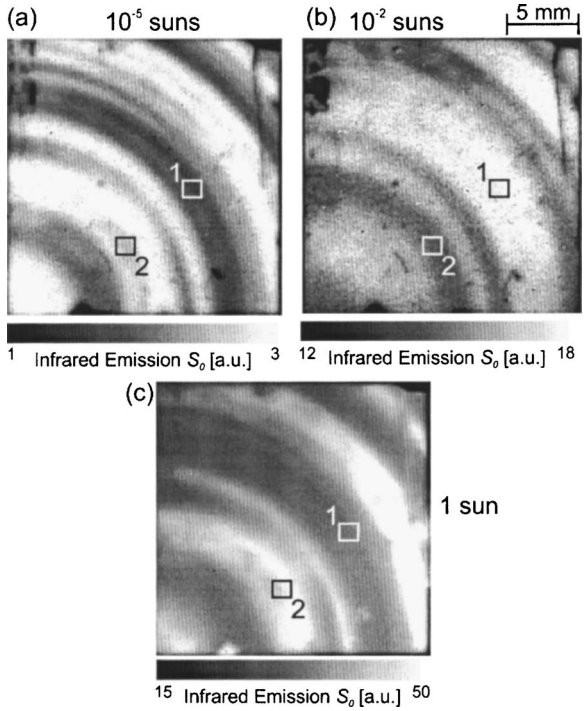

FIG. 1. Infrared emission S_0 of a Cz–Si wafer obtained using lock-in infrared emission measurements at 70 °C. The mappings are measured at three different illumination intensities: (a) 10^{-5} suns, (b) 10^{-2} suns, and (c) 1 sun.

dependent apparent lifetime curves measured at the positions marked as 1 and 2 in Fig. 1. The two curves have been measured in 1×1 mm^2 areas with the lowest (circles, Position 1) and highest (triangles, Position 2) lifetimes at 1 sun illumination intensity. These curves clearly reveal a strong increase of the apparent lifetime τ_a with decreasing injection level, which is typically observed when minority-carrier trapping occurs. Note that a similar dependence has also been measured on silicon nitride passivated *p*-type silicon wafers without the presence of trapping centers. This effect was attributed to the storage of electrons in the space-charge region produced by the highly positively charged silicon nitride film.[12] We can exclude this effect here as we are only studying *n*-type silicon.

If minority-carrier trapping centers are present in a sample, charge neutrality requires an increased density of majorities, leading to an additional steady-state infrared

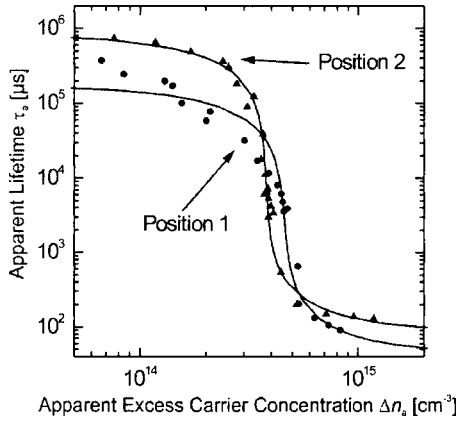

FIG. 2. Exemplary injection-dependent lifetime curves $\tau_a(\Delta n_a)$ at two different positions (marked in Figs. 1 and 3) of a Cz–Si wafer obtained using lock-in infrared emission measurements at 70 °C.

emission signal. Assuming *n*-type silicon, the infrared emission signal becomes

$$S_0 = m\left(1+\frac{\alpha_n}{\alpha_p}\right)\Delta nW + m\frac{\alpha_n}{\alpha_p}n_tW, \tag{2}$$

where n_t equals the concentration of trapped carriers. For *p*-type material, the correction factor α_n/α_p in the second term of Eq. (2) drops out. In the following, we assume *n*-type material.

We apply a simple single-level trap model to the ILM technique, which was suggested by Hornbeck and Haynes[13] and applied by Macdonald *et al.*[4] to the QSSPC technique. Following the line of arguments given in Ref. 4, we find for the apparent lifetime

$$\tau_a = \tau_r\left[1+\frac{N_t}{\Delta n + N_t(\tau_t/\tau_d)}\frac{\alpha_n}{\alpha_p+\alpha_n}\right], \tag{3}$$

where τ_r is the recombination lifetime. As our measurements are performed under low-level injection conditions, τ_r does not depend on the injection level. Furthermore, the apparent carrier concentration Δn_a is related to the actual excess carrier concentration Δn via[14]

$$\Delta n_a = \frac{\tau_a}{\tau_r}\Delta n. \tag{4}$$

In order to image the trap density N_t, we have developed the following three-step evaluation procedure:

(i) For $\Delta n \gg N_t$, Eq. (3) simplifies to $\tau_a=\tau_r$. In this case, our camera signal directly gives the spatially resolved recombination lifetime $\tau_r(x,y)$.

(ii) For $\Delta n \ll N_t$, Eq. (3) simplifies to

$$\frac{\tau_t}{\tau_d} = \frac{\tau_r}{\tau_a-\tau_r}\frac{\alpha_n}{\alpha_p+\alpha_n}. \tag{5}$$

Hence, using the result for $\tau_r(x,y)$ from Step (i), we obtain the spatially resolved ratio $\tau_t/\tau_d(x,y)$.

(iii) Knowing τ_r and τ_t/τ_d, we determine the trap density $N_t(x,y)$ using the expression

$$N_t = \Delta n_a\frac{1-\tau_r/\tau_a}{\dfrac{\alpha_n}{\alpha_p+\alpha_n}+(\tau_t/\tau_d)(\tau_a/\tau_r-1)}. \tag{6}$$

This equation is directly derived from Eqs. (3) and (4) and it is valid within the entire injection range, where trapping effects impact the lifetime. To calculate N_t from our measurements, we use a Δn_a value close to the maximum negative slope of the measured $\tau_a(\Delta n_a)$ dependence in a double-logarithmic plot (see Fig. 2) as this gives the smallest uncertainty in N_t. Note that in a double-logarithmic plot of $\tau_a(\Delta n_a)$, the Δn_a value corresponding to the maximum negative slope shifts linearly with N_t.

Finally, we generate a mapping of the trap center energy level using[13]

$$E_t - E_v = kT\ln\left[\frac{N_v}{N_t}\left(\frac{\tau_d}{\tau_t}\right)\right], \tag{7}$$

where N_v is the effective density of states in the valence band.

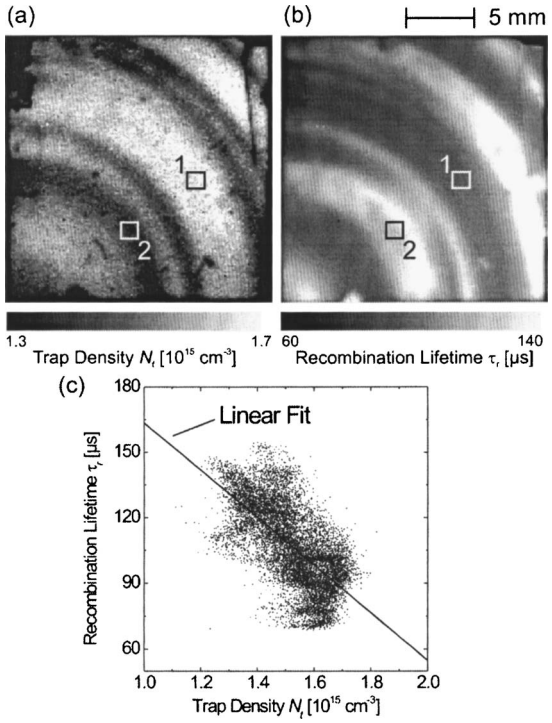

FIG. 3. (a) Trap density N_t mapping of a Cz–Si wafer measured using the ITM method. (b) Mapping of the recombination lifetime τ_r of the same sample measured using the ILM technique. A clear anticorrelation between the trap density and the recombination lifetime mapping is found. (c) Plot of the recombination lifetime τ_r vs the trap density N_t at each point of the mappings. The linear fit results in a negative slope of $-(1.09\pm0.01)\times10^{-19}$ s cm^{-3}.

Applying our three-step evaluation procedure to the experimental data of the Cz–Si wafer shown in Fig. 1 results in the spatially resolved trap density image shown in Fig. 3(a). As can be seen from Fig. 2, the approximation $\tau_r=\tau_a$ is well satisfied for the highest measured injection levels. Fitting Eqs. (3) and (4) to the experimental data shown in Fig. 2 yields trap densities N_t of 1.7×10^{15} cm^{-3} and 1.4×10^{15} cm^{-3} for Positions 1 and 2, respectively. The trap density $N_t(x,y)$ calculated by the ITM method ranges from 1.3 to 1.7×10^{15} cm^{-3}. The area-average trap density shown in Fig. 3(a) is $\langle N_t\rangle=(1.53\pm0.11)\times10^{15}$ cm^{-3}. It is interesting to note that, as can be seen from Fig. 3(a), there exists a correlation between areas of higher trap densities and striation patterns. Also, a clear anticorrelation between the trap density in Fig. 3(a) and the recombination lifetime mapping in Fig. 3(b) is found. In order to quantitatively underline this anticorrelation, we plot in Fig. 3(c) the recombination lifetime τ_r versus the trap density N_t at each point of the mappings. A linear fit results in a negative slope of $-(1.09\pm0.01)\times10^{-19}$ s cm^{-3}.

An image of the trap energy level E_t corresponding to the N_t mapping shown in Fig. 3(a) reveals a very homogeneous distribution around $E_t=E_v+(0.587\pm0.005)$ eV. The homogeneity in E_t over the measured area is better than 1%, whereas the homogeneity in N_t is ~7%, suggesting that only one type of trap is measured. It has been shown recently that oxygen-related traps can be present in large concentrations in Cz–Si.[14] The fact that the energy level of the trapping center is very deep is surprising at first glance. One reason might be that the deep traps are heavily charged, repelling majority carriers and therefore having only little recombination activity. However, the deepness of the traps might also be a result of the oversimplification of the trap model.[14] Theoretical studies aiming at an improved trapping model are currently under way in our lab.

In conclusion, we have introduced a lock-in infrared camera trap mapping technique for the investigation of spatially distributed minority-carrier trapping centers. Using an evaluation procedure based on a single-level trap model, we were able to generate mappings of the trap density and the energy level. An application of the technique to Cz–Si wafers showed strong inhomogeneities in the trap densities, whereas the energy levels of the trapping centers were found to be almost independent of position. We observed an anticorrelation between trap densities and recombination lifetimes in Cz–Si showing typical striation patterns. The latter finding suggests that trapping and recombination centers are of similar origin in this particular sample.

Funding was provided by the State of Lower Saxony.

[1] R. Bube, *Photoelectronic Properties of Semiconductors* (Cambridge University Press, Cambridge, UK, 1992).
[2] M. Kunst and G. Beck, J. Appl. Phys. **60**, 3558 (1986).
[3] T. Tiedje, J. Habermann, R. Francis, and A. Gosh, J. Appl. Phys. **54**, 2499 (1983).
[4] D. Macdonald and A. Cuevas, Appl. Phys. Lett. **74**, 1710 (1999).
[5] R. Sinton and A. Cuevas, Appl. Phys. Lett. **69**, 2510 (1996).
[6] M. Bail, J. Kentsch, R. Brendel, and M. Schulz, *Proceedings of the 28th IEEE Photovoltaics Conference*, Anchorage, Alaska (IEEE, New York, 2000), pp. 99–103.
[7] J. Isenberg, S. Riepe, S. Glunz, and W. Warta, J. Appl. Phys. **93**, 4268 (2003).
[8] P. Pohl and R. Brendel, in *Proceedings of the 19th European Photovoltaic Solar Energy Conference* (WIP, Paris, 2004), pp. 46–49.
[9] O. Breitenstein and M. Langenkamp, *Lock-in Thermography, Basics and Use for Functional Diagnostics of Electronic Components* (Springer, New York, 2003).
[10] D. Schroder, R. Thomas, and J. Schwartz, IEEE Trans. Electron Devices **25**, 254 (1978).
[11] T. Lauinger, J. Schmidt, A. Aberle, and R. Hezel, Appl. Phys. Lett. **69**, 1232 (1996).
[12] M. Bail, M. Schulz, and R. Brendel, Appl. Phys. Lett. **82**, 757 (2003).
[13] J. Hornbeck and J. Haynes, Phys. Rev. **97**, 311 (1955).
[14] J. Schmidt, K. Bothe, and R. Hezel, Appl. Phys. Lett. **80**, 4395 (2002).